

YOUNG CLUSTER BERKELEY 59 : PROPERTIES, EVOLUTION AND STAR FORMATION

NEELAM PANWAR ¹, A. K. PANDEY ², MANASH R. SAMAL ³, PAOLO BATTINELLI ⁴, K. OGURA ⁵, D. K. OJHA ⁶, W. P. CHEN ³, H. P. SINGH ¹

¹Department of Physics & Astrophysics, University of Delhi, Delhi-110007, India

²Aryabhata Research Institute of Observational Sciences (ARIES), Nainital - 263129, India

³Graduate Institute of Astronomy, National Central University 300, Jhongli City, Taoyuan County - 32001, Taiwan

⁴INAF, Osservatorio Astronomico di Roma Viale del Parco Mellini 84, I-00136 Roma, Italy

⁵Kokugakuin University, Higashi, Shibuya-ku, Tokyo - 1508440, Japan

⁶Tata Institute of Fundamental Research, Mumbai (Bombay) - 400 005, India

ABSTRACT

Berkeley 59 is a nearby (~ 1 kpc) young cluster associated with the Sh2-171 HII region. We present deep optical observations of the central $\sim 2.5 \times 2.5$ pc² area of the cluster, obtained with the 3.58-m Telescopio Nazionale Galileo. The $V/(V-I)$ color-magnitude diagram manifests a clear pre-main-sequence (PMS) population down to $\sim 0.2 M_{\odot}$. Using the near-infrared and optical colors of the low-mass PMS members we derive a global extinction of $A_V = 4$ mag and a mean age of ~ 1.8 Myr, respectively, for the cluster. We constructed the initial mass function and found that its global slopes in the mass ranges of $0.2 - 28 M_{\odot}$ and $0.2 - 1.5 M_{\odot}$ are -1.33 and -1.23 , respectively, in good agreement with the Salpeter value in the solar neighborhood. We looked for the radial variation of the mass function and found that the slope is flatter in the inner region than in the outer region, indicating mass segregation. The dynamical status of the cluster suggests that the mass segregation is likely primordial. The age distribution of the PMS sources reveals that the younger sources appear to concentrate close to the inner region compared to the outer region of the cluster, a phenomenon possibly linked to the time evolution of star-forming clouds is discussed. Within the observed area, we derive a total mass of $\sim 10^3 M_{\odot}$ for the cluster. Comparing the properties of Berkeley 59 with other young clusters, we suggest it resembles more to the Trapezium cluster.

Keywords: stars : formation - stars : pre-main-sequence - ISM : globules HII regions - open cluster: initial mass function; star formation.

1. INTRODUCTION

Since most stars in the Galaxy are formed in clusters (e.g., Lada & Lada 2003), the processes responsible for cluster formation are important to include any consideration of the mechanisms of star formation. Despite recent advances that have been made in this field, including observational and theoretical work focusing on the different stages of star formation, a number of mechanisms remain unclear. It is still debated whether star formation is a fast, dynamic process (Elmegreen 2000, 2007; Hartmann & Burkert 2007a) or slow (Tan et al. 2006) proceeding for at least several dynamical timescales. Similarly, since most of the massive stars form in clusters it is still unclear whether initial mass function (IMF) is universal (Bastian et al. 2010; Offner et al. 2014) or it depends on the environments as observed in some extreme starburst galaxies and young massive clusters (Stolte et al. 2005; van Dokkum & Conroy 2010; Lu et al. 2013). Massive stars potentially influence their surroundings through their en-

ergetic radiation and stellar winds by regulating the dynamics, density and temperature distribution of the gas (e.g., Koenig et al. 2008; Ojha et al. 2011; Deharveng et al. 2012; Samal et al. 2014; Panwar et al. 2014; Jose et al. 2016). Hence these could be dominating factors in shaping the fundamental properties of the cluster such as IMF and total star formation efficiency. Also the evolution of circumstellar disks around the young stars can be affected (e.g. Dib et al. 2010, and references therein).

Observations of very young clusters, before they dynamically relaxed, can provide some indications of the initial conditions of their formation. Therefore, a careful characterization of the basic properties of clustered systems at their early evolutionary stages is essential to put constraints on the formation of such systems.

Berkeley 59 (Be 59) is a young cluster (~ 2 Myr; Pandey et al. 2008) located at the centre of the Cepheus OB4 stellar association and is surrounded by the HII region Sh2-171 (Yang & Fukui 1992). It is a relatively

nearby cluster (distance ~ 1 kpc) showing variable reddening with $E(B - V)$ ranging from 1.4 to 1.8 mag (Majaess et al. 2008; Pandey et al. 2008). It contains several massive stars (spectral type from O7 to B5) (Kun et al. 2008; Majaess et al. 2008; Skiff 2014; Maíz Apellániz et al. 2016) which are still associated with the natal molecular clouds making it one of the potential nearby massive clusters. Yang & Fukui (1992) observed two dense molecular clumps ('C1' and 'C2') at the western side of the Be 59 using the $J = 1 - 0$ lines of ^{12}CO and ^{13}CO emission. They suggested that the dense gas is in contact with the HII region Sh2-171, and the ionization front (IF) is driving shocks into the clumps and a new generation of stars may be triggered to form from the compressed gas layer. Rosvick & Majaess (2013) studied the region using WISE data and identified a small group of embedded stars (RA: 00h 00m 46s, DEC: $+67^\circ 32' 59''$, J2000.0) which resides in a cloud within the clump 'C2'. On the basis of velocity studies Yang & Fukui (1992) found that the local standard-of-rest velocity (V_{LSR}) of the clump 'C2' (-16 km/s) matches that of Be 59 (-15.7 km/s) derived from observations of member stars (Liu et al. 1989). Hence, the clump appears to be physically related with Be 59.

Though the cluster has been investigated by several authors at optical bands (Majaess et al. 2008; Pandey et al. 2008; Lata et al. 2011; Eswaraiah et al. 2012), most of these studies were limited to the high to intermediate mass stars only. Pandey et al. (2008) identified intermediate mass population of young stellar objects (YSOs) in the region using near-infrared 2MASS and slitless grism $H\alpha$ data. However, their optical photometry could detect stars upto $V \sim 18.5$ mag corresponding to $\sim 1.5 M_\odot$ at the adopted distance and extinction of the cluster. Recently, Koenig et al. (2012); Rosvick & Majaess (2013); Getman et al. (2017) identified candidate YSOs in the region, however, no adequate attention has been paid to the characterization of low-mass young stellar population of the cluster by using deep optical photometric data. Since the low-mass stars constitute the majority of the stellar population in the Galaxy, the low-mass stellar content and its IMF are essential to understand the nature of the star formation process and the properties of stellar systems.

In this paper, we present new observations of the central area of Be 59 at optical wavelengths obtained with the 3.58-m Telescopio Nazionale Galileo (TNG). These new observations are the deepest to date for this region and allow us to assess the stellar contents of the cluster down to $0.2 M_\odot$, and provide a better analysis of its properties and mass function, understanding on the dynamical status, and insight into its formation. In Section 2, we present the optical observations, the data reduction and the archive datasets utilized in this study. In Sec-

tion 3, the identification of PMS population, extinction measurements, IMF and the mass-segregation and star-formation associated to the cluster are discussed. Finally, the results of the present work are summarized in Section 4.

2. OBSERVATIONS AND DATA REDUCTION

Figure 1 shows the color-composite image (red: $4.6 \mu\text{m}$ from WISE, green: $2.2 \mu\text{m}$ from 2MASS, blue: $0.65 \mu\text{m}$ from DSS2) of the Be 59 region. The boxes 'A' and 'B' ($\sim 8'.6 \times 8'.6$ each) represent the area covered by our optical observations. 'C1' and 'C2' represent the locations of the peaks of the molecular clumps (cf. Yang & Fukui 1992).

In Fig. 1, a clustering of stellar sources is clearly apparent at the center of the image. The figure also displays several red WISE sources, indicating the presence of a likely young stellar population, still deeply embedded in the molecular cloud. The diffuse optical emission is mainly seen at the center of the cluster indicating low-extinction at the central direction compared to the outskirts where molecular cloud is present. In the present work, we used optical observations of 'region A' to examine the cluster properties of Be 59, while observations of 'region B' are used to understand the origin of star formation observed towards C2.

2.1. Optical Observations

The VI observations of the two regions of the cluster Be 59 (see Fig. 1), region 'A' (RA: 00h 02m 14.0s, DEC: $+67^\circ 25' 08''.0$) and region 'B' (RA: 00h 01m 08.0s, DEC: $+67^\circ 33' 03''.0$), and a control field having the same area (centered at RA: 00h 09m 48.0s, DEC: $+68^\circ 07' 58''.0$) were obtained by using the Device Optimized for the LOw RESolution (DOLORES) instrument mounted on the TNG. DOLORES is a focal reducer instrument equipped with a 2048×2048 square pixel CCD detector, with a plate scale of $0.252''/\text{pixel}$ and a field of view (FoV) of $8.6' \times 8.6'$. During the observations the average seeing was $\sim 1''$. The details of the observations are given in table 1.

A number of bias and flat frames were also taken during the observations. The pre-processing of the data frames was done by using various tasks available under the IRAF data reduction software package. The fringing patterns were present in the I band frames which were removed by using the *rmfringe* task available in IRAF. The photometric measurements of the stars were performed by using DAOPHOT – II software package (Stetson 1987). The point spread function (PSF) was obtained for each frame by using several uncontaminated stars and the PSF photometry of all the sources was obtained using the ALLSTAR task in IRAF (e.g., Ojha et al. 2009; Jose et al. 2017).

The instrumental magnitudes were converted to the

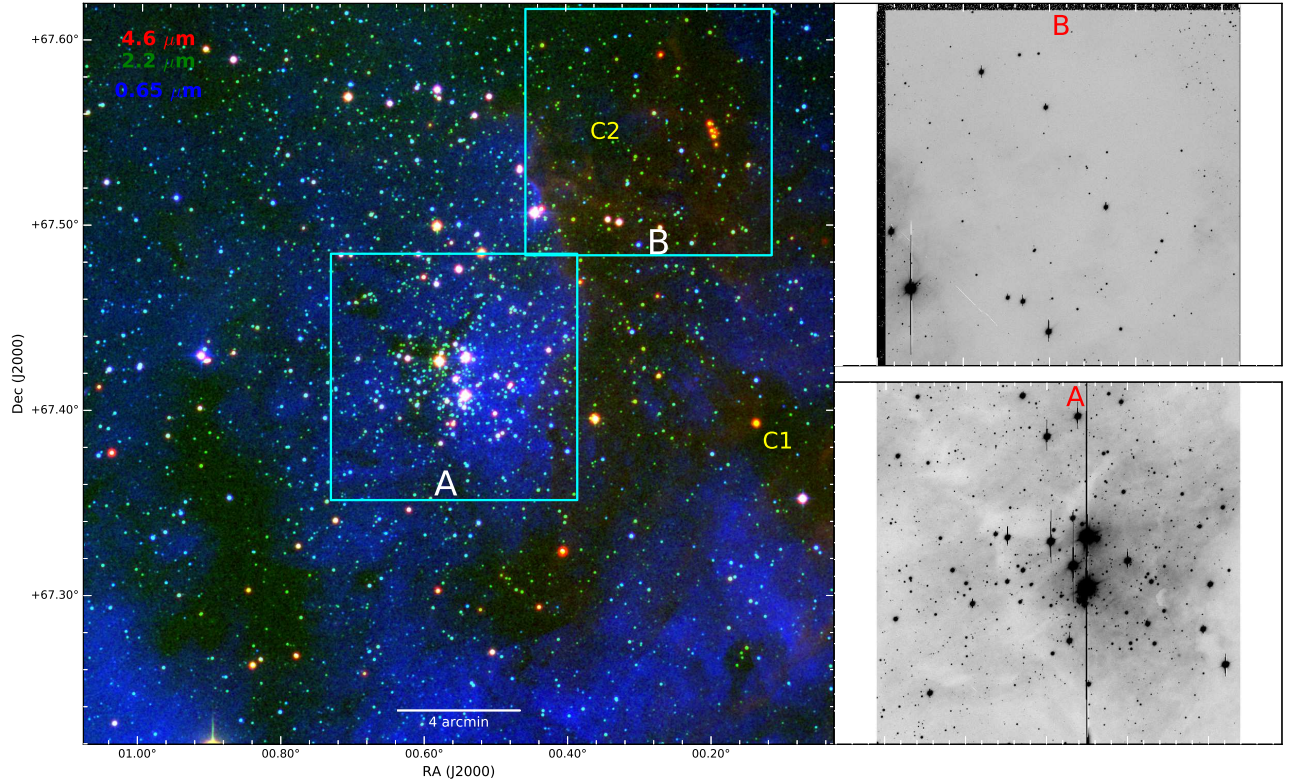


Figure 1. Three-color image (red: $4.6 \mu\text{m}$, green: $2.2 \mu\text{m}$, blue: $0.65 \mu\text{m}$) of the Be 59 region. The two boxes (marked as ‘A’ and ‘B’) represent the DOLORES observations. ‘C1’ and ‘C2’ are the locations of the two dense clumps identified by [Yang & Fukui \(1992\)](#). The optical images of the regions A and B are shown in grey scale also.

Table 1. Log of observations

$\alpha_{(2000)}$ (h:m:s)	$\delta_{(2000)}$ (d:m:s)	Filter & Exposure(sec) \times no. of frames	Date of observations (yr-mm-dd)	Regions
00:02:14.0	+67:25:08.0	V:275 \times 6;I:275 \times 6	2009-10-12	Region ‘A’
00:02:14.0	+67:25:08.0	V:60 \times 3;I:60 \times 3	2010-08-31	Region ‘A’
00:01:08.0	+67:33:03.0	V:275 \times 6,60 \times 3;I:275 \times 6,6s \times 3	2010-08-31	Region ‘B’
00:09:48.0	+68:07:58.0	V:275 \times 6,60 \times 3;I:275 \times 6,60 \times 3	2010-08-31	Field region

standard values by using the secondary standards from [Lata et al. \(2012\)](#). The photometric accuracies depend on the brightness of the stars. We finally consider only those sources with uncertainty < 0.2 mag in V and I . Our data (detection limit, $V \sim 24$ mag) are ~ 5.5 mag deeper than that of [Pandey et al. \(2008, \$V \sim 18.5\$ mag\)](#).

2.2. Data Completeness

To derive cluster properties, it is necessary to take into account the incompleteness in the observed data that may occur for various reasons, e.g., crowding of the stars, diffuse emission, variable extinction etc. A quantitative evaluation of the completeness of the photometric data with respect to the brightness and the position on a given frame is necessary to convert the observed luminosity function (LF) to a true LF. We used the ADDSTAR rou-

tine of *DAOPHOT – II* to determine the completeness factor (CF). The procedure has been outlined in detail in our earlier works (e.g., [Pandey et al. 2001](#); [Chauhan et al. 2011](#)). Briefly, we randomly added the artificial stars to both V and I images in such a way that they have similar geometrical locations. The luminosity distribution of artificial stars is chosen in such a way that more stars are inserted towards the fainter magnitude bins. The frames were reduced by using the same procedure used for the original frame. The ratio of the number of stars recovered to that added in each magnitude interval gives the CF as a function of magnitude. The minimum value of the CF of the pair (i.e., the V and I band observations), given in [Table 2](#), is used to correct the data for incompleteness. The incompleteness of the data increases with increasing magnitude as expected. As can be seen from the table, in

Table 2. Completeness factor of the photometric data in the cluster region and control field.

V range (mag)	cluster region	control field
17.0 - 17.5	1.00	1.00
17.5 - 18.0	1.00	1.00
18.0 - 18.5	1.00	1.00
18.5 - 19.0	1.00	1.00
19.0 - 19.5	0.99	0.99
19.5 - 20.0	0.98	0.98
20.0 - 20.5	0.97	0.97
20.5 - 21.0	0.95	0.96
21.0 - 21.5	0.93	0.96
21.5 - 22.0	0.92	0.95
22.0 - 22.5	0.90	0.92
22.5 - 23.0	0.87	0.90
23.0 - 23.5	0.83	0.87
23.5 - 24.0	0.81	0.84

V-band the completeness of the cluster region is better than 80% level at ~ 23.5 mag.

2.3. YSOs from Infra-red and X-ray Observations

During their early phase, stars possess circumstellar disks and hence show the excess emission in the IR wavelengths. The IR excess property of YSOs can be used to identify and classify them in different evolutionary classes, i.e., Class 0, Class I, Class II and Class III (André 1995). Whereas Class ‘II’ sources are surrounded by optically thick disks and also exhibit near infrared (NIR) to far infrared (FIR) excess emission, Class ‘III’ sources have optically thin disks or they may be disk anemic, so possess little or no excess in IR (Lada 1987; André 1995; Lada et al. 2006; Luhman 2012). Hence, IR observations are less sensitive to identify Class III sources. However, Class II, Class III sources (referred as PMS stars) are often strong X-ray emitters and very luminous in the X-ray regime compared to their main-sequence (MS) counterparts (e.g., Feigelson & Montmerle 1999; Getman et al. 2005; Preibisch & Feigelson 2005; Güdel et al. 2007; Getman et al. 2012). Hence, X-ray surveys of star forming regions are used to uncover YSO populations. Particularly, for the detection of disk anemic YSOs, i.e., Class III sources, X-ray observations complement the YSO sources obtained from IR observations and a better census of the low-mass stellar content of clusters can be achieved (e.g., Preibisch & Feigelson 2005; Feigelson et al. 2013; Broos et al. 2013; Pandey et al. 2013a, 2014; Preibisch et al. 2017). Recently, Getman et al. (2017) carried out the *Star Formation in Nearby Clouds (SF_NCs)* project to provide detailed studies of the young stellar populations and star cluster formation in nearby star forming regions (SFRs) including Be 59. They identified ~ 700 young stars using 2MASS (JHK_s), *Spitzer*-IRAC (3.6 μ m, 4.5 μ m) and X-ray data from

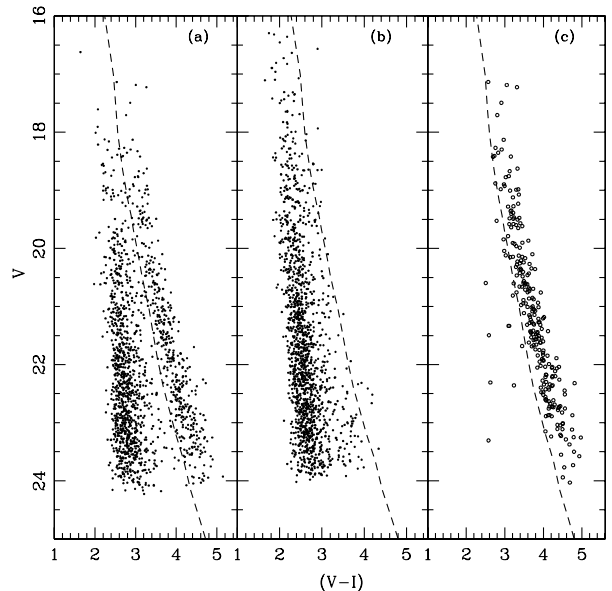


Figure 2. Color-magnitude diagrams (CMDs) for the stars in (a) region A, and (b) the control field. The dashed line is drawn to tentatively separate the PMS population from the field stars. (c) CMD for the known candidate YSOs from Getman et al. (2017).

Chandra space telescope, which were classified as sources with disks, without disks and probable members. Our optical observations are well within their area of study. Hence, we have used their YSO catalog in this work to guide our analysis and, in particular, to identify the PMS stars of the cluster as well as to characterize the cluster. While NIR, MIR and X-ray observations are suitable to identify PMS stars, the characterization of these stars (e.g., age and mass determinations) can be done more accurately by optical observations as PMS stars possess little or no circumstellar emission at optical wavelengths. Owing to large off axis beam of *Chandra*, we checked these likely members for the counterparts of our optical dataset with a less stringent matching radius of 3 arcsec. In a few cases, where there were more than one source within the matching radius, we considered the closest one as the best match (e.g., Panwar et al. 2017). This search revealed possible optical counterparts to 257 (72 %) sources in the region A.

3. RESULTS & DISCUSSION

3.1. Identification of PMS members of the cluster

The color magnitude diagram (CMD) is an ideal tool to study the evolutionary stages of the member stars of the cluster. However, CMDs can be contaminated severely by the field population along the line of sight (e.g., Sung & Bessell 2010; Da Rio et al. 2010; Chauhan et al. 2011; Sung et al. 2013; Pandey et al. 2013b). The cluster population can be distinguished from the general Galactic

population along the line of sight through a comparison of the CMDs of the cluster region and the control field (e.g., Brandner et al. 2008; Sharma et al. 2008; Gennaro et al. 2011; Hayes et al. 2015). In Fig 2a and 2b, we show the V vs. $(V - I)$ CMDs for the stars in the cluster region and control field, respectively. As can be seen, the cluster PMS population clearly stands out in the cluster CMD compared to the control field CMD. There is a clear color gap between the likely PMS sources of the cluster and that of the field stars towards that direction. Comparing the cluster and field regions, we consider those stars that lie right of the dashed curve (see Fig. 2a) as the PMS population of the cluster. To further confirm the PMS zone, we compare the distribution of the previously identified YSOs (i.e, YSOs identified by using *Spitzer* and X-ray observations; see Sec. 2.3) on the CMD (see Fig. 2c) to the distribution of the field stars. In doing so, we found that most of the YSOs are actually located right of the dashed line, reinforcing our hypothesis that the contamination due to field stars in the PMS population of the Be 59 region is insignificant. Comparing the number of field stars to that of stars located right of the dashed line, the level of contamination by field stars in our PMS sample is less than 3%.

3.2. Extinction measurement

Previous studies have determined reddening ($E(B - V)$) of Be 59 in the range of 1.4 to 1.8 mag from the optical measurements of a few bright stars (Pandey et al. 2008; Majaess et al. 2008). Since, the current data-set extends substantially deeper than the previous surveys and the PMS content is clearly identified. Here, we utilize the near-infrared colors of the low-mass content of the cluster to derive its extinction, since the near-infrared colors of low-mass stars are less sensitive to the change in spectral types. To do so, we selected all the PMS sources that lie to the right of the dashed line in the optical CMD (see Fig. 2a), then searched for their NIR counterparts within a $1''$ and followed the same procedure as outlined in Sec. 2.3. The NIR colors of these sources are shown in Fig. 3 (upper left panel). As can be seen from this $(J - H)$ vs. $(H - K)$ color-color diagram, a majority of them are located in the reddened MS zone (i.e, the zone between the two reddening vectors), and only a few sources show characteristics of infrared excess (i.e, those sources located beyond the right reddening vector), indicating that the likely excess emission due to the circumstellar disk is less or minimum for a majority of the sources (for details on NIR color-color diagram, see Ojha et al. 2009, and references therein). The fluxes in the redder infrared bands may be contaminated by the infrared excess emission arising from the circumstellar disk. However, it is generally considered that among near-infrared bands the effects of the excess emission in J-band is minimum (e.g.,

Meyer et al. 1997; Luhman et al. 2003b). Even though only a few PMS sources show infrared excess in the $(J - H)$ vs. $(H - K)$ color-color diagram, we select only those sources that do not show characteristics of infrared excess in order to minimize the effect of excess emission on extinction. Figure 3 (middle panel), shows the J vs. $(J - H)$ diagram of these PMS sources. Over-plotted solid curves are the 1 Myr and 10 Myr isochrones from Baraffe et al. (1998) with zero reddening and at the adopted distance (1 kpc). In both the plots the isochrones and photometric magnitudes are converted into the CIT system by using the transformation equations from Carpenter (2001). As can be seen from the figure, at the low-mass end the PMS isochrones are almost vertical in the J vs. $(J - H)$ diagram, particularly below $J=14$ mag. As the color change for the low-mass PMS objects ($J > 14$ mag) due to age variations within the expected age range of 1 - 10 Myr is minor, so de-reddening is possible with a unique solution for each star. To get better statistics on the extinction, we use a slightly relaxed criterion by selecting those sources that lie below the reddening vector (shown as an arrow) originating at $J = 13.5$ mag (instead of $J = 14$ mag) and $(J - H) = 0.68$ mag, i.e, the sources within the shaded area in the plot. We then derived the color excess of these selected sources by tracing them back to the vertical line of the plot along the reddening vector, then converted the color excess to the $A_V (=9.1 \times E(J - H))$, for $R_V=3.1$ value using the reddening law of Cohen et al. (1981) which is in the CIT system.

The distribution of the derived visual extinction values is shown in Fig. 3 (lower panel). The peak and dispersion of the visual extinction distribution as estimated from a Gaussian fit are 4.0 mag and 1.2 mag, respectively. This mean visual extinction corresponds to an $E(B - V)=1.3$ mag. This is in very good agreement with the extinction estimation based on the bright stars by previous authors. For the further analyses, we use $A_V= 4$ mag as the mean visual extinction of the region.

3.3. Age/Mass of the YSOs in the cluster region

The ages of the massive stars are difficult to estimate as they quickly arrive on the main sequence while the low-mass stars are still on their PMS tracks. Thus ages of young clusters are typically derived from post-main-sequence evolutionary tracks for the massive members showing significant evolution, or based on theoretical PMS isochrones for low-mass contracting population. Here, we rely on a sample of young stars (the PMS sources identified in Sec. 3.1) to derive the age of Be 59.

Fig. 4 represents the optical $V/(V - I)$ CMD for our PMS stars in the region A. The 2 Myr main sequence (MS) by Girardi et al. (2002) as well as the PMS isochrones for 1 and 5 Myr having the solar metallicity

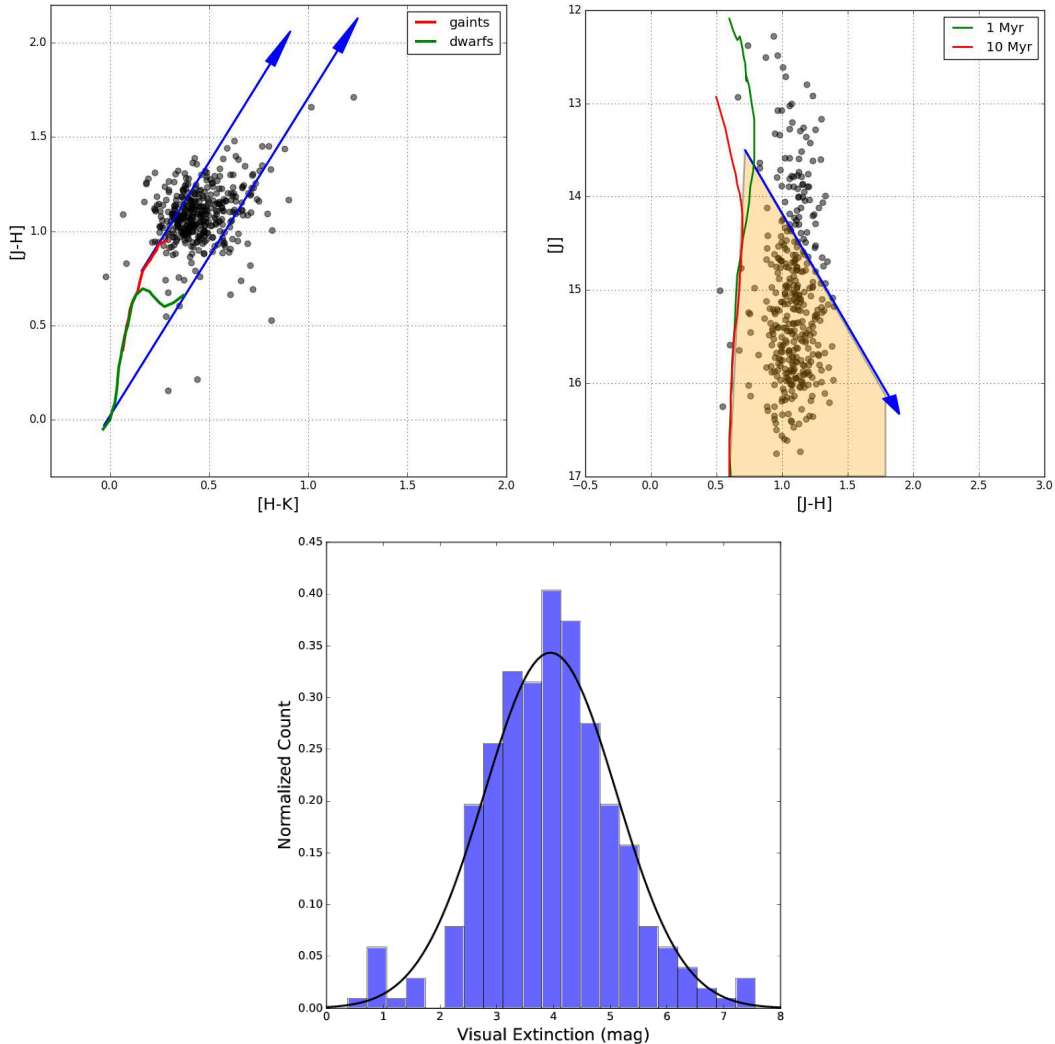


Figure 3. Upper left panel : 2MASS ($J - H$) vs. ($H - K$) color-color diagram of the PMS stars. The red solid line show typical colors of giants from [Bessell & Brett \(1988\)](#). The solid green curve shows the intrinsic colors of the MS stars from [Bessell & Brett \(1988\)](#). The blue arrows indicate the reddening vectors according to the extinction laws of [Cohen et al. \(1981\)](#). Upper right panel: J vs. ($J - H$) color-magnitude diagram of the PMS stars without IR-excess. Over-plotted are 1 and 10 Myr isochrones from [Baraffe et al. \(1998\)](#) for the adopted distance (1 kpc) and zero reddening. The shaded area represents the sample selected for extinction measurements. The arrow is the reddening vector according to the extinction law of [Cohen et al. \(1981\)](#). Bottom panel: Distribution of the derived visual extinction of the PMS population. The solid curve represents the Gaussian fit to the distribution.

by [Siess et al. \(2000\)](#) are also plotted¹. The isochrones are shifted for the adopted distance (1 kpc) and reddening, $E(B - V) = 1.3$ mag. To determine the age and mass of each star, we downloaded a large number of PMS isochrones from [Siess et al. \(2000\)](#) for 0.1 to 10 Myr with

¹ Here, we used [Siess et al. \(2000\)](#) isochrones because the evolutionary models of [Baraffe et al. \(1998\)](#) is limited to 1 Myr and lack isochrones for masses above $1.3 M_{\odot}$. Consequently, the median age of the cluster can only be constrained to < 1 Myr. On the other hand, [Siess et al. \(2000\)](#) models extend to younger ages than those of [Baraffe et al. \(1998\)](#), thus provide us with additional information on the age of the cluster population, as well as means to compare our results with previous results of Be 59, where the authors have used the Siess models to derive the membership, age, and mass function (e.g., [Pandey et al. 2008](#); [Eswaraiah et al. 2012](#)).

an interval of 0.1 Myr from their web interface. We then interpolated each isochrone to make them to be more continuous curves. Finally, we assign the age and mass to a star corresponding to the closest isochrone on the CMD. The age and mass of the YSOs are given in [Table 3](#). Only a portion of [Table 3](#) is given here and the complete table is available in the electronic version.

The age distribution derived for the PMS sources is shown in [Figure 5](#). As one can see from the figure, the distribution shows a scatter in age primarily between 0.5 to 5 Myr. The mean age of the cluster population is $\sim 1.8 \pm 0.9$ Myr, which is in good agreement with that

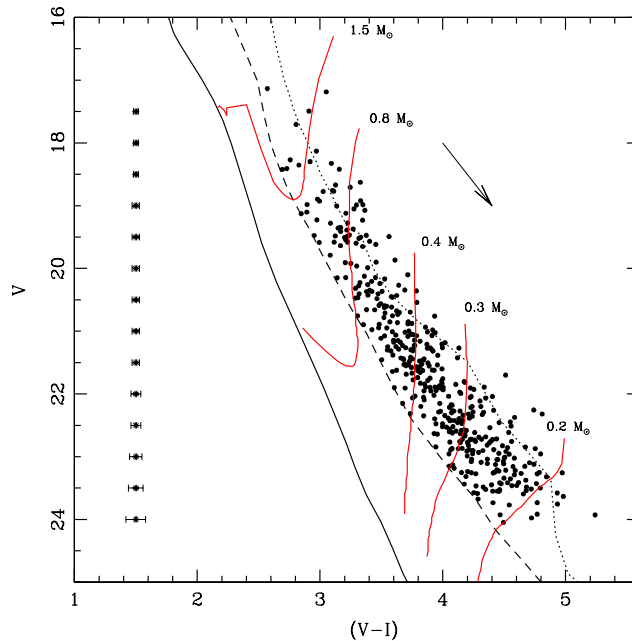


Figure 4. Color-magnitude diagram for the PMS sources in the present work. The 2 Myr MS (continuous curve) by [Girardi et al. \(2002\)](#) as well as the PMS isochrones for 1 and 5 Myr (dotted and dashed curves, respectively) having solar metallicity by [Siess et al. \(2000\)](#) are also plotted. The isochrones are shifted for the adopted distance (1 kpc) and reddening ($E(B - V)=1.3$ mag). The arrow represents the reddening vector of $A_V=1$ mag. The average error in $(V - I)$ color as a function of magnitude is shown on the left-hand side.

obtained by [Pandey et al. \(2008\)](#).

In the case of young clusters this type of age spread is common and may be due to the combined effect of differential reddening, circumstellar disk extinction, binarity, variability and/or different evolutionary stages of the cluster members. Since, in the V vs. $(V - I)$ CMD, the reddening vector is nearly parallel to the isochrones, a small differential reddening (i.e., $\Delta A_V = 1$ mag in the present case) may not significantly affect the age estimation. Though the circumstellar disk may affect the age and mass determination of YSOs in IR CMDs, its effect should be minimal in optically visible sources such as sources with optically thin disks (e.g., [Jose et al. 2013](#)). In fact as one can see from Fig. 3 (upper panel), most of the PMS sources do not possess optically thick disk at NIR bands. A binary system appears brighter and, consequently will be assigned a younger age on the basis of the CMD. For example, in the case of equal-mass binaries, a cluster is expected to show a sequence which is shifted by 0.75 mag upwards. The effect of binarity can be more prominent in somewhat evolved clusters (~ 10 Myr) in which many member stars are in Henyey track and so the isochrones are closer to each other, whereas in the case of very young clusters the isochrones are more separated, hence the effect of binarity on age estimation will be less compared to the natural age spread of

the stars in the clusters (e.g., [Sicilia-Aguilar et al. 2005](#); [Panwar et al. 2017](#)). Similarly though, most of the young stars (T-Tauri stars) show variability at optical bands (e.g., [Herbst et al. 1994](#); [Rodríguez-Ledesma et al. 2010](#); [Lata et al. 2016](#)), however, as demonstrated by [Burningham et al. \(2005\)](#), due to variability the location of objects in the CMD tend to move parallel to the isochrones, resulting in little effect on the age estimation (see also discussion in [Scholz 2012](#)).

Despite of the low differential reddening and presence of large number of disk-less sources in the cluster, some degree of age spread due to the combination of the above factors is expected, but since the observed spread in color among the PMS members is larger than their typical uncertainties due to photometric colors (see Fig. 4), we considered that PMS stars are likely at different evolutionary stages.

We consider that the errors associated with the determination of age and mass are mainly of two kinds; random errors in photometry, and systematic errors due to different theoretical evolutionary tracks. We estimated the effect of random errors by propagating them to the observed estimations of V , $(V-I)$ and $E(V-I)$ by assuming a normal error distribution and by using Monte Carlo simulations (see e.g., [Chauhan et al. 2009](#)). Since we have used the same evolutionary model (i.e., [Siess et al. 2000](#))

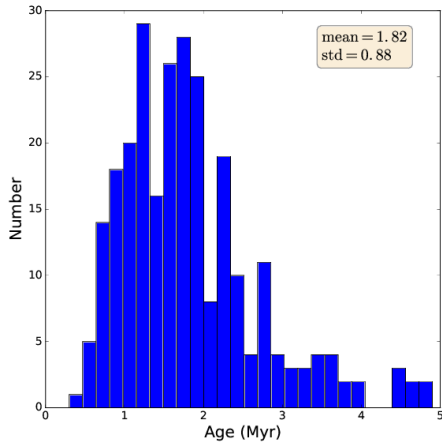


Figure 5. Age distribution for the PMS stars with mass $> 0.3 M_{\odot}$.

to calculate the age/mass for all the PMS stars, the results should not be affected by systematic errors.

3.4. Initial Mass Function and Mass of the Cluster

The IMF is the distribution of the masses of stars at the time of a star formation event. Young clusters are preferred sites for IMF studies as their mass functions (MFs) can be considered as IMFs, since they are too young to lose a significant number of members either due to dynamical evolution or stellar evolution. The variation of the IMF gives clues to the physical conditions of star formation processes (e.g., Bate 2009). The IMF is defined as the number of stars per unit logarithmic mass interval, and is generally represented by a power law with the slope,

$$\Gamma = d \log N(\log m) / d \log m,$$

where $N(\log m)$ is the number of stars per unit logarithmic mass interval. The classical value derived by Salpeter (1955) is $\Gamma = -1.35$ for the mass range $0.4 < M/M_{\odot} \leq 10$.

Here, we used the optical CMD to count the number of stars in different mass bins, which is shown in Fig. 4 along with isochrones and evolutionary tracks. To make corrections to the data sample for incompleteness which may be due to various reasons, e.g., crowding of the stars, we used the ADDSTAR routine of *DAOPHOT-II* to determine the CF as described in Sec. 2.1. The IMF of the PMS stars was obtained by counting the number of stars in different mass bins and correcting for incompleteness (for details see Pandey et al. 2008; Jose et al. 2008). Fig. 6 shows the MF of the cluster region A in the mass range $0.2 \leq M/M_{\odot} \leq 28$. We note our data is sensitive to the mass-range $0.2 - 1.5 M_{\odot}$. Since most of the bright stars ($V < 18$ mag with the corresponding mass $> 1.5 M_{\odot}$) were saturated in our observations, the data for higher masses ($> 1.5 M_{\odot}$) have been taken from Pandey et al.

(2008).

As can be seen from the figure, the mass function rises up to $0.3 M_{\odot}$. Deep infrared observations will be more efficient to shed light on the sub-stellar population of the cluster and its IMF. Nonetheless, we note, the low-mass IMF has been investigated for a number of other star-forming regions, and in some cases the results are similar to the IMF derived here. For example, a variety of photometric and spectroscopic surveys have been completed in the extremely dense Trapezium cluster and the intermediate density cluster IC 348 by multiple authors (Hillenbrand & Carpenter 2000; Muench et al. 2002, 2003; Slesnick et al. 2004; Lucas et al. 2005). All of them found an increasing mass functions to a maximum at $0.1 - 0.3 M_{\odot}$ before declining in the brown dwarf regime. These results are very different from the mass function derived for the Taurus star-forming region (characterized by its low gas and stellar densities), which peaks at $0.8 M_{\odot}$ (Briceño et al. 2002; Luhman et al. 2003a; Luhman 2004).

A single slope for the IMF in the mass range $0.2 \leq M/M_{\odot} \leq 28$ can be fitted with $\Gamma = -1.33 \pm 0.11$, which is nearly equal to the Salpeter value (-1.35). If we fit a single slope to the data in the mass range $0.2 \leq M/M_{\odot} \leq 1.5$, the resultant Γ value is -1.23 ± 0.26 , which is comparable to the Salpeter value. We note, Pandey et al. (2008) estimated a slope of -1.01 in the mass range $2.5 - 28 M_{\odot}$, which could be due to combination of low statistics of stars at high-mass end, small mass range and different area used by them.

It is difficult to make an accurate estimate of the cluster mass without knowing all the low-mass members. We can however make a relatively good estimate from the present data as they reach down to $0.2 M_{\odot}$. Most of the observations of the high-mass SFRs in our Galaxy are consistent with an IMF that declines below $0.2 M_{\odot}$ (e.g., Luhman 2007; Andersen et al. 2008; Oliveira et al. 2009; Sung & Bessell 2010; Neichel et al. 2015; Jose et al. 2017). Thus the contribution below it is not expected to substantially alter the estimate of the total mass of the cluster if we assume that the cluster contains stars down to $0.08 M_{\odot}$. Adopting -1.33 as the slope of the mass function, we estimate the total mass of the cluster as $\sim 950 M_{\odot}$ by integrating the mass function between 0.2 and $28 M_{\odot}$. The total number of stars in the cluster down to $0.2 M_{\odot}$ is estimated to be ~ 1500 . The stellar density profile of the cluster based on the optical data suggests that most of the stars are located within $5 - 8$ arcmin radial distance from the center of the cluster (Pandey et al. 2008). Although our data represent majority of the cluster members, however, we emphasize that the estimated mass is a lower-limit to the actual total mass of the cluster and only represents the mass within the central part of radius ~ 4 arcmin (~ 1.2 pc).

Table 3. Magnitudes, mass and age of the PMS stars. Complete table is available in an electronic form.

Id	RA (J2000)	DEC (J2000)	V \pm eV	I \pm eI	Mass \pm error in Mass (M_{\odot})	Age \pm error Age (Myr)
1	0.668875	67.343697	20.90 \pm 0.02	17.54 \pm 0.02	0.73 \pm 0.16	4.50 \pm 0.33
2	0.411083	67.346443	19.57 \pm 0.02	16.16 \pm 0.02	0.62 \pm 0.10	0.76 \pm 0.05
3	0.461458	67.347725	22.34 \pm 0.02	18.33 \pm 0.03	0.34 \pm 0.04	2.40 \pm 0.10
...

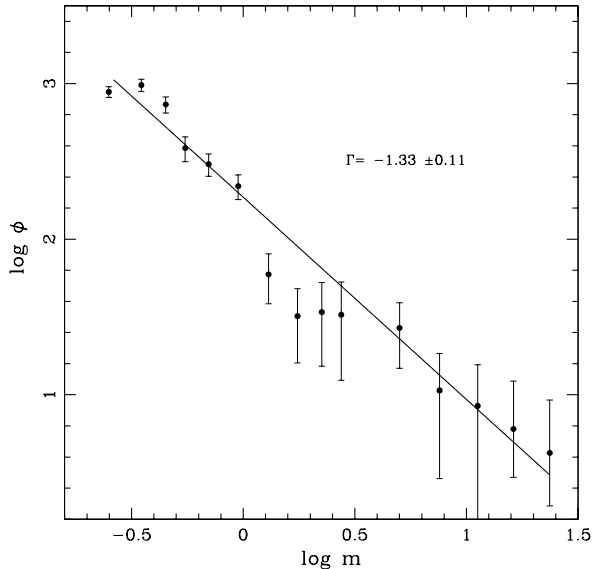


Figure 6. The IMF in the region derived from the optical data. The ϕ represents $N/d \log m$. The error bars represent the $\pm\sqrt{N}$ errors. The continuous line shows the weighted least-squares fit in the mass ranges described in the text. The value of the slope obtained is given in the figure.

3.5. Mass Segregation

The concentration of massive cluster members at the center and lower mass members at larger radii is commonly referred as mass-segregation in clusters. Whether mass segregation is primordial or dynamical, is an important constraint on theories of massive star formation as well as cluster formation and evolution. The competitive accretion theory (Bonnell et al. 2001; Bonnell & Bate 2006) suggests that protostars in the dense central regions of a young star cluster can accrete more material than those in the outskirts, therefore primordial mass segregation would be a natural outcome of massive star formation. However, mass segregation can occur dynamically (Kroupa et al. 2001; McMillan et al. 2007). In this scenario massive stars form elsewhere in the cluster but sink to the cluster center through dynamical interaction with low-mass stars. The dynamical evolution drives the system towards equipartition, the natural result of this being that the lower-mass stars attain higher velocities, hence occupy larger orbits around the cluster centre. In

turn, the higher-mass stars will sink towards the cluster centre.

In Be 59, as discussed in Pandey et al. (2008), the high-mass stars are more centrally concentrated than their lower mass siblings. Although, the issue of mass segregation has been extensively investigated in clusters by focusing on high-mass stars (e.g., Chen et al. 2007; Pang et al. 2013; Lim et al. 2013; Wang et al. 2014), the possibility of differential mass segregation among low-mass stars has been rarely discussed (e.g., Andersen et al. 2011). Some theories concerning the formation of very low-mass stars suggest such objects may have a greater velocity dispersion than their higher mass siblings and hence be less spatially concentrated in a cluster (e.g., Sterzik & Durisen 2003).

In this work, we investigated the mass segregation by looking at the radial variation of the IMF of low-mass stars. To do so, we divided the cluster into two radial bins of width 2 arcmin and derived the IMFs using the stars in the mass range 0.3 - 1.5 M_{\odot} . Figure 7 shows the IMFs of the cluster in these two bins. As can be seen from the figure, the slope of the IMF in the inner bin (i.e., between 0-2 arcmin) is clearly flatter than the outer bin (i.e., between 2-4 arcmin), although the fluctuation of the data points is rather large due to the low statistics of stars. Since the mass function slopes differ from each other by more than 4σ uncertainty, where σ is the error associated to the slope, we view this trend as an evidence for mass segregation in the cluster.

The time-scale for the onset of significant dynamical mass segregation is comparable to the dynamical relaxation time of the cluster. We estimate the dynamical relaxation time t_{relax} for the cluster:

$$t_{relax} = \frac{N}{8 \ln N} \times t_{cross},$$

where $t_{cross} = \frac{R}{\sigma_v}$ is the crossing time, R is the size of the cluster, N is the total number of stars and σ_v is the velocity dispersion of the stars (Bonnell & Davies 1998). From the CO observation of Be 59 (Liu et al. 1988), the velocity dispersion of the molecular gas is $\sim 1.4 \text{ km s}^{-1}$. In the absence of kinematic information of the stellar members of the cluster we use the velocity dispersion of CO gas to roughly estimate the relaxation time. Considering $R \sim 2.6 \text{ pc}$, $\sigma_v \sim 1.4 \text{ km s}^{-1}$ and $N \sim 1500$, we obtain $t_{relax} \sim 4.5 \text{ Myr}$ for Be 59. As the cluster age is $\sim 1.8 \text{ Myr}$, no significant mass segregation is expected from two-body dynamical interactions. The cluster still

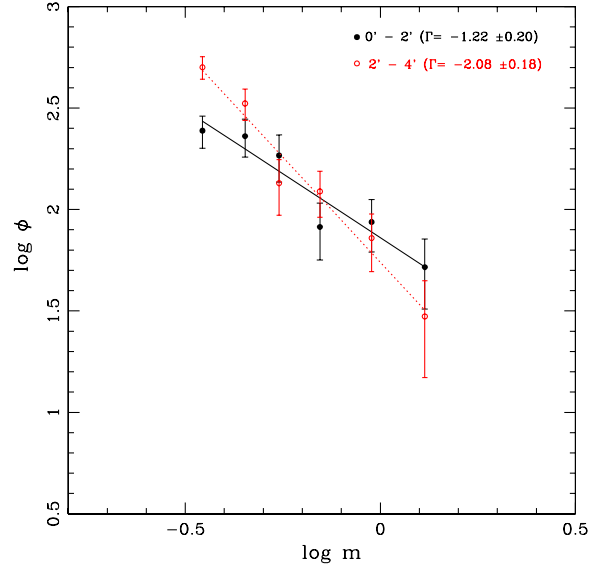


Figure 7. IMFs for the low-mass stars lying within 0-2 arcmin and 2-4 arcmin from the cluster center. The ϕ represents $N/d \log m$. The solid lines show the weighted least square fit to the data.

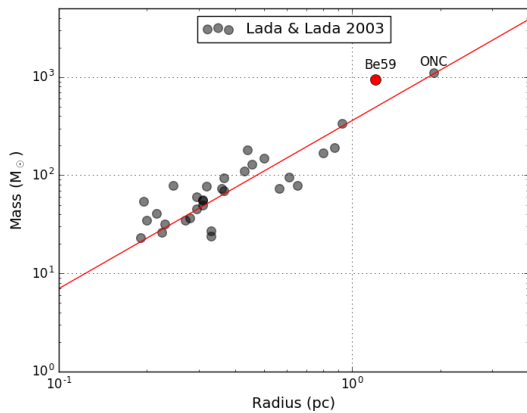


Figure 8. Comparison of Be 59 with the other nearby clusters. The cluster sample is from Lada & Lada (2003). The location of Be 59 and ONC is marked.

retains a significant amount of molecular gas and cold dust components (see discussion in Pandey et al. 2008; Yang & Fukui 1992) that are usually thought to impede the process of dynamical mass segregation. From the above evidences, we argue that the mass segregation is likely primordial, although precise kinematic measurements of stellar members would shed more light on this issue.

3.6. Comparison to other nearby clusters

With the total mass of $\sim 1000 M_{\odot}$, the age ~ 2 Myr and the stellar population containing early-mid O-type stars, Be 59 presents a nearby, rich and partially embedded young cluster. Therefore, it is worthwhile to compare

the properties of Be 59 with those of the nearby embedded clusters in our Galaxy. Figure 8 shows the data sample (black dots) of embedded clusters from the Lada & Lada (2003) with known sizes and masses. This data set is limited to embedded clusters within 2 kpc from the Sun, and, like Be 59, they are far enough away from the Galactic centre and the spiral arms. In Fig. 8 the solid line shows the relation, $\text{mass} \propto \text{radius}^{1.7}$, obtained by Pfalzner (2011) by using the Lada & Lada (2003) sample. As can be seen, Be 59 follows the above mass-radius relation well. Interestingly it resembles Orion Nebula Cluster (ONC). ONC is one of the nearest young clusters with approximately $1000 M_{\odot}$ of stars (Hillenbrand 1997; Da Rio et al. 2010). The most massive star of Trapezium, θ Ori C, is of spectral type O7V (Stahl et al. 2008). The second massive is of O9.5V, and the rest two are of B0-B1. Reggiani et al. (2011) calculated the age of ONC based on the Siess et al. (2000) evolutionary models and found a mean age of around 2.2 Myr (see also Jeffries et al. 2011, who reached a nearly similar conclusion).

Compared to ONC, Be 59 contains ~ 1500 stars, with the total stellar mass of $\sim 1000 M_{\odot}$ and a mean age of ~ 1.8 Myr. Also the spectral types of the four bright members (lying within 0.24 pc from the center) in the Be 59 are similar to those of the Trapezium system (see Table 4). So we argue that Be 59 is an ONC-like cluster located in the the Galaxy at the distance of ~ 1 kpc.

3.7. Clues on cluster formation

Spatial variation in stellar ages with respect to the cluster radius is a footprint of how star formation progressed throughout space and time. Along with kinematics of the

Table 4. Four massive members of the cluster Be 59

Name	distance from the cluster center (in pc)	V mag	Spectral Type	Reference
BD +66 1675	0.17	9.08	O7	Majaess et al. (2008)
BD +66 1674	0.24	9.60	B0	Majaess et al. (2008)
LS I +67 9	0.02	11.30	B0.5	Majaess et al. (2008)
TYC 4026-0424-1	0.23	11.81	O9	Maíz Apellániz et al. (2016)

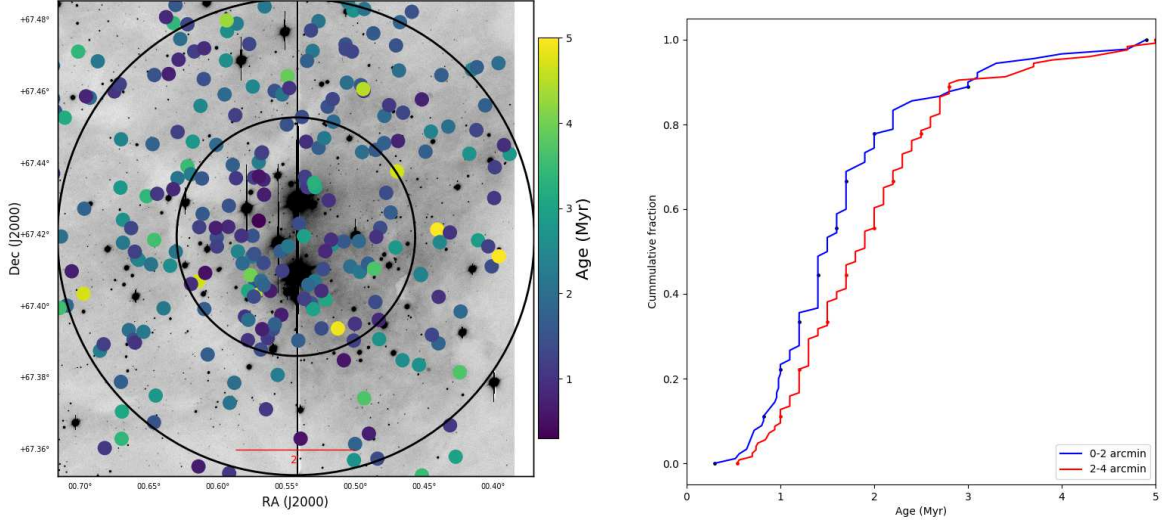


Figure 9. Left panel: Age distribution of low-mass stars. The inner and outer circles present radii of 2 arcmin and 4 arcmin, respectively. Right panel: KS test on the age distribution of the stars within 0 - 2 arcmin and 2 - 4 arcmin from the cluster center.

stars, it traces the duration of the star formation process, therefore helps to constrain theoretical models and improve our understanding on the cluster formation. For example, in ONC, [Fűrész et al. \(2008\)](#) and [Tobin et al. \(2009\)](#) showed that the radial velocities of most of the optically studied stars are consistent with those of the molecular gas, which led them to suggest that both the gas and stars in ONC are collapsing towards the central regions. They argue that ONC is kinematically young and yet not dynamically relaxed and in a state of dynamical collapse. Similarly, a decade ago [Hartmann & Burkert \(2007b\)](#) suggested that the Orion A cloud is undergoing gravitational collapse on large scales, and is producing ONC through the focusing effects of gravity. Their suggestion is that the effects of the global gravity result in ever increasing densities with runaway contraction in subregions and a small number of stars apparently older than a few Myr found in or projected upon star-forming regions may be a signature of the cloud evolution. The idea of large-scale gravitational collapse is also consis-

tent with observed column density probability density functions ([Ballesteros-Paredes et al. 2011](#)). If the cluster forming clumps are in a state of hierarchical runaway global gravitational contraction then one would expect older stars at the outskirts of the cluster than near the center (e.g., see discussion in [Vázquez-Semadeni et al. 2017](#)). In fact, based on photometric analyses such a core-halo age gradient has been seen in the ONC: the PMS stars in the cluster core appear younger and thus were formed later than the PMS stars in the cluster halo ([Getman et al. 2014](#)), consistent with the age segregation noticed in the ONC by [Hillenbrand \(1997\)](#) three decades ago.

Figure 9 shows the spatial distribution of the stellar ages of the low-mass (0.3 to $1.5 M_{\odot}$) stars in Be 59, in which the blue to yellow colors represent the age sequence from young to old. As can be seen from the figure, the inner region of the cluster shows some degree of segregation of younger stars (i.e., redder sources) compared to the outer region. A Two-sample Kolmogorov

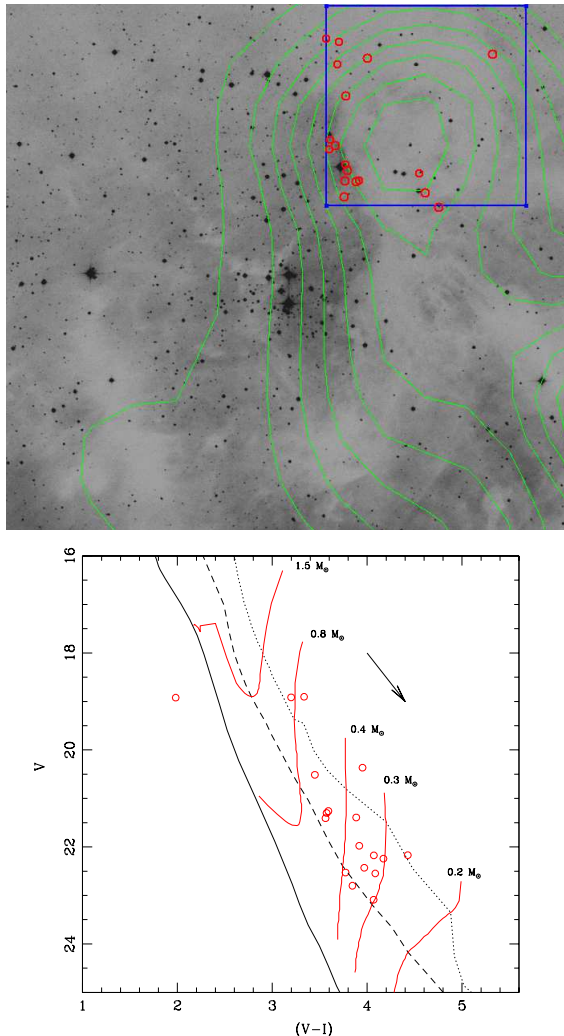


Figure 10. Upper panel: The spatial distribution of the YSOs (red circles) in region B along with the cloud dust emission at 870 GHz observed with *Planck* (green contours). Lower panel: The locations of the YSOs on the V vs. $(V - I)$ CMD. The isochrones and evolutionary tracks have the same meaning as in Fig. 4.

- Smirnov (KS) test confirms that the age distributions of the stars within 0 to 2 arcmin and 2 to 4 arcmin are distinct with a p-value of 0.01. Since our age analysis is based only on photometric data, a further investigation is certainly needed. In any case, if this ‘age segregation’ is fully confirmed, this may have significant implications on the formation of Be 59.

3.8. Triggered star formation around Be 59

The Be 59 cluster lies in the center of the HII region Sh2-171, also known as W1. Bright-rimmed clouds BRC 1, BRC 2 and BRC 3 are to the west, north and east of the cluster, respectively (cf. Sugitani et al. 1991). BRCs are thought to arise under the impact of UV photons from nearby massive stars on pre-existing

dense molecular material (Lefloch & Lazareff 1994; Miao et al. 2009), leading to the formation of a new generation of stars by a radiatively-driven implosion (Ogura et al. 2002; Morgan et al. 2004; Samal et al. 2012; Panwar et al. 2014; Sharma et al. 2016). Yang & Fukui (1992) found two dense molecular clouds (‘C1’ and ‘C2’) on the western side of Be 59 (see Fig. 1). One of the clumps C1 harbours BRC 1. Ogura et al. (2002) detected six $H\alpha$ stars in the vicinity of BRC 1 may be low-mass stars of the second generation. A small elongated aggregate of stars inside the clump C2 has been noticed by Rosvick & Majaess (2013). In the present work, we have studied the region B which encloses C2. Our optical observations detected counterparts of a few young stars (Getman et al. 2017) in region B. The spatial distribution of these stars along with the cloud dust emission at 870 GHz is shown in Fig. 10 (left panel) and their locations on the V vs. $(V - I)$ CMD are shown in Fig. 10 (right panel). In Fig. 10 (right panel), the PMS isochrones of 1 and 5 Myr from Siess et al. (2000), corrected for the adopted distance and reddening of the cluster, are also plotted. As can be seen from Fig. 10, these stars are mostly located towards the south of the clump which is close to the cluster. We note these stars are located well within the cluster radius of Be 59, thus, these stars could be part of the cluster. We assessed the age and mass of these YSOs using the same approach as discussed in Sec. 3.3. We estimated a mean age of these stars as ~ 2.5 Myr. This mean age is normally higher than that of the cluster (i.e., 1.8 Myr). We note that adoption of a higher extinction value would yield even older ages for these stars. Thus, probably being older (or of similar age) than the members of the cluster, they are unlikely to be formed as a result of the triggering by the massive stars of Be 59. Our present data is not sensitive enough to pin-down star formation within the clump C2. Deep infra-red photometric and spectroscopic observations would shed more light on the star formation and evolutionary stages of the YSOs within C2.

4. CONCLUSIONS

We present the V and I band observations of the central region of the cluster Berkeley 59 using the 3.58-m Telescopio Nazionale Galileo, which are the deepest ($V \sim 24$ mag) observations so far for the region. The optical V vs. $(V-I)$ CMD for the stars in the region shows a well defined PMS population. We estimated the extinction of $A_V = 4$ mag towards the cluster using the NIR ($J - H$) and $(H - K)$ colours of the probable PMS low-mass stars. We assessed the age and mass of the PMS population identified in the present work by comparing their locations on the CMD with the evolutionary models of various ages by Siess et al. (2000). This yield a mean age of ~ 1.8 Myr for the cluster, which is comparable

to that of previous studies. We find that the slopes of the IMF for the stars in the cluster region are -1.33 and -1.23 in the mass ranges 0.2 - 28 M_{\odot} and 0.2 - 1.5 M_{\odot} , respectively, consistent with the other Galactic clusters. To study the radial variation of the mass function within the cluster, we constructed the IMFs in two regions: inner (0 - 2 arcmin) and outer (2 - 4 arcmin). The slope of the IMF is flatter in the inner region compared to that of the outer region, indicating that there are relatively more low-mass stars in the outer region as compare to the inner region. Since it is a young cluster (< 2 Myr), still associated with the parental cloud, the observed mass-segregation is likely primordial. The age distribution of the PMS sources reveals that most of the younger sources are centrally distributed and older stars tend to be in the outer region of the cluster. Comparing the mass-radius relation of Be 59 with other young clusters, it seems to resemble the Trapezium cluster. Our present data do not show signs of triggering and age sequence towards the clump C2. The deep infra-red observations of the clump can shed more light on the embedded young stellar population and its properties.

We are thankful to the anonymous referee for valuable comments. NP acknowledges the financial support from the Department of Science & Technology, INDIA, through INSPIRE faculty award IFA-PH-36 at University of Delhi. This work is based on observations made with the Italian Telescopio Nazionale Galileo (TNG) operated on the island of La Palma by the Fundacin Galileo Galilei of the INAF (Istituto Nazionale di Astrofisica) at the Spanish Observatorio del Roque de los Muchachos of the Instituto de Astrofisica de Canarias. This publication makes use of data from the Two Micron All Sky Survey (a joint project of the University of Massachusetts and the Infrared Processing and Analysis Center/ California Institute of Technology, funded by the National Aeronautics and Space Administration and the National Science Foundation), archival data obtained with the *Spitzer Space Telescope* (operated by the Jet Propulsion Laboratory, California Institute of Technology, under contract with the NASA).

REFERENCES

- Andersen, M., Meyer, M. R., Greissl, J., & Aversa, A. 2008, *ApJL*, 683, L183
- Andersen, M., Meyer, M. R., Robberto, M., Bergeron, L. E., & Reid, N. 2011, *A&A*, 534, A10
- André, P. 1995, *Astrophysics & Space Science*, 224, 29
- Ballesteros-Paredes, J., Vázquez-Semadeni, E., Gazol, A., et al. 2011, *MNRAS*, 416, 1436
- Baraffe, I., Chabrier, G., Allard, F., & Hauschildt, P. H. 1998, *A&A*, 337, 403
- Bastian, N., Covey, K. R., & Meyer, M. R. 2010, *ARA&A*, 48, 339
- Bate, M. R. 2009, *MNRAS*, 392, 1363
- Bessell, M. S., & Brett, J. M. 1988, *PASP*, 100, 1134
- Bonnell, I. A., & Bate, M. R. 2006, *MNRAS*, 370, 488
- Bonnell, I. A., Clarke, C. J., Bate, M. R., & Pringle, J. E. 2001, *MNRAS*, 324, 573
- Bonnell, I. A., & Davies, M. B. 1998, *MNRAS*, 295, 691
- Brandner, W., Clark, J. S., Stolte, A., et al. 2008, *A&A*, 478, 137
- Briceño, C., Luhman, K. L., Hartmann, L., Stauffer, J. R., & Kirkpatrick, J. D. 2002, *ApJ*, 580, 317
- Broos, P. S., Getman, K. V., Povich, M. S., et al. 2013, *ApJS*, 209, 32
- Burningham, B., Naylor, T., Littlefair, S. P., & Jeffries, R. D. 2005, *MNRAS*, 363, 1389
- Carpenter, J. M. 2001, *AJ*, 121, 2851
- Chauhan, N., Pandey, A. K., Ogura, K., et al. 2011, *MNRAS*, 415, 1202
- . 2009, *MNRAS*, 396, 964
- Chen, L., de Grijs, R., & Zhao, J. L. 2007, *AJ*, 134, 1368
- Cohen, J. G., Persson, S. E., Elias, J. H., & Frogel, J. A. 1981, *ApJ*, 249, 481
- Da Rio, N., Robberto, M., Soderblom, D. R., et al. 2010, *ApJ*, 722, 1092
- Deharveng, L., Zavagno, A., Anderson, L. D., et al. 2012, *A&A*, 546, A74
- Dib, S., Shadmehri, M., Padoan, P., et al. 2010, *MNRAS*, 405, 401
- Elmegreen, B. G. 2000, *ApJ*, 530, 277
- . 2007, *ApJ*, 668, 1064
- Eswaraiah, C., Pandey, A. K., Maheswar, G., et al. 2012, *MNRAS*, 419, 2587
- Feigelson, E. D., & Montmerle, T. 1999, *ARA&A*, 37, 363
- Feigelson, E. D., Townsley, L. K., Broos, P. S., et al. 2013, *ApJS*, 209, 26
- Fűrész, G., Hartmann, L. W., Megeath, S. T., Szentgyorgyi, A. H., & Hamden, E. T. 2008, *ApJ*, 676, 1109
- Gennaro, M., Brandner, W., Stolte, A., & Henning, T. 2011, *MNRAS*, 412, 2469
- Getman, K. V., Broos, P. S., Kuhn, M. A., et al. 2017, *ApJS*, 229, 28
- Getman, K. V., Feigelson, E. D., Grosso, N., et al. 2005, *ApJS*, 160, 353
- Getman, K. V., Feigelson, E. D., & Kuhn, M. A. 2014, *ApJ*, 787, 109
- Getman, K. V., Feigelson, E. D., Sicilia-Aguilar, A., et al. 2012, *MNRAS*, 426, 2917
- Girardi, L., Bertelli, G., Bressan, A., et al. 2002, *A&A*, 391, 195
- Güdel, M., Skinner, S. L., Mel'Nikov, S. Y., et al. 2007, *A&A*, 468, 529
- Hartmann, L., & Burkert, A. 2007a, *ApJ*, 654, 988
- . 2007b, *ApJ*, 654, 988
- Hayes, C. R., Friel, E. D., Slack, T. J., & Boberg, O. M. 2015, *AJ*, 150, 200
- Herbst, W., Herbst, D. K., Grossman, E. J., & Weinstein, D. 1994, *AJ*, 108, 1906
- Hillenbrand, L. A. 1997, *AJ*, 113, 1733
- Hillenbrand, L. A., & Carpenter, J. M. 2000, *ApJ*, 540, 236
- Jeffries, R. D., Littlefair, S. P., Naylor, T., & Mayne, N. J. 2011, *MNRAS*, 418, 1948
- Jose, J., Herczeg, G. J., Samal, M. R., Fang, Q., & Panwar, N. 2017, *ApJ*, 836, 98
- Jose, J., Kim, J. S., Herczeg, G. J., et al. 2016, *ApJ*, 822, 49
- Jose, J., Pandey, A. K., Ojha, D. K., et al. 2008, *MNRAS*, 384, 1675
- Jose, J., Pandey, A. K., Samal, M. R., et al. 2013, *MNRAS*, 432, 3445
- Koenig, X. P., Allen, L. E., Gutermuth, R. A., et al. 2008, *ApJ*, 688, 1142

- Koenig, X. P., Leisawitz, D. T., Benford, D. J., et al. 2012, *ApJ*, 744, 130
- Kroupa, P., Aarseth, S., & Hurley, J. 2001, *MNRAS*, 321, 699
- Kun, M., Kiss, Z. T., & Balog, Z. 2008, *Star Forming Regions in Cepheus*, ed. B. Reipurth, 136
- Lada, C. J. 1987, in *IAU Symposium*, Vol. 115, *Star Forming Regions*, ed. M. Peimbert & J. Jugaku, 1–17
- Lada, C. J., & Lada, E. A. 2003, *ARA&A*, 41, 57
- Lada, C. J., Muench, A. A., Luhman, K. L., et al. 2006, *AJ*, 131, 1574
- Lata, S., Pandey, A. K., Chen, W. P., Maheswar, G., & Chauhan, N. 2012, *MNRAS*, 427, 1449
- Lata, S., Pandey, A. K., Maheswar, G., Mondal, S., & Kumar, B. 2011, *MNRAS*, 418, 1346
- Lata, S., Pandey, A. K., Panwar, N., et al. 2016, *MNRAS*, 456, 2505
- Lefloch, B., & Lazareff, B. 1994, *A&A*, 289, 559
- Lim, B., Chun, M.-Y., Sung, H., et al. 2013, *AJ*, 145, 46
- Liu, T., Janes, K. A., & Bania, T. M. 1989, *AJ*, 98, 626
- Liu, T., Janes, K. A., Bania, T. M., & Phelps, R. L. 1988, *AJ*, 95, 1122
- Lu, J. R., Do, T., Ghez, A. M., et al. 2013, *ApJ*, 764, 155
- Lucas, P. W., Roche, P. F., & Tamura, M. 2005, *MNRAS*, 361, 211
- Luhman, K. L. 2004, *ApJ*, 617, 1216
- . 2007, *ApJS*, 173, 104
- . 2012, *ARA&A*, 50, 65
- Luhman, K. L., Briceño, C., Stauffer, J. R., et al. 2003a, *ApJ*, 590, 348
- Luhman, K. L., Stauffer, J. R., Muench, A. A., et al. 2003b, *ApJ*, 593, 1093
- Maíz Apellániz, J., Sota, A., Arias, J. I., et al. 2016, *ApJS*, 224, 4
- Majaess, D. J., Turner, D. G., Lane, D. J., & Moncrieff, K. E. 2008, *Journal of the American Association of Variable Star Observers (JAAVSO)*, 36, 90
- McMillan, S. L. W., Vesperini, E., & Portegies Zwart, S. F. 2007, *ApJL*, 655, L45
- Meyer, M. R., Calvet, N., & Hillenbrand, L. A. 1997, *AJ*, 114, 288
- Miao, J., White, G. J., Thompson, M. A., & Nelson, R. P. 2009, *ApJ*, 692, 382
- Morgan, L. K., Thompson, M. A., Urquhart, J. S., White, G. J., & Miao, J. 2004, *A&A*, 426, 535
- Muench, A. A., Lada, E. A., Lada, C. J., & Alves, J. 2002, *ApJ*, 573, 366
- Muench, A. A., Lada, E. A., Lada, C. J., et al. 2003, *AJ*, 125, 2029
- Neichel, B., Samal, M. R., Plana, H., et al. 2015, *A&A*, 576, A110
- Offner, S. S. R., Clark, P. C., Hennebelle, P., et al. 2014, *Protostars and Planets VI*, 53
- Ogura, K., Sugitani, K., & Pickles, A. 2002, *AJ*, 123, 2597
- Ojha, D. K., Tamura, M., Nakajima, Y., et al. 2009, *ApJ*, 693, 634
- Ojha, D. K., Samal, M. R., Pandey, A. K., et al. 2011, *ApJ*, 738, 156
- Oliveira, J. M., Jeffries, R. D., & van Loon, J. T. 2009, *MNRAS*, 392, 1034
- Pandey, A. K., Nilakshi, Ogura, K., Sagar, R., & Tarusawa, K. 2001, *A&A*, 374, 504
- Pandey, A. K., Samal, M. R., Chauhan, N., et al. 2013a, *New Astronomy*, 19, 1
- Pandey, A. K., Samal, M. R., Yadav, R. K., et al. 2014, *New Astronomy*, 29, 18
- Pandey, A. K., Sharma, S., Ogura, K., et al. 2008, *MNRAS*, 383, 1241
- Pandey, A. K., Eswaraiah, C., Sharma, S., et al. 2013b, *ApJ*, 764, 172
- Pang, X., Grebel, E. K., Allison, R. J., et al. 2013, *ApJ*, 764, 73
- Panwar, N., Chen, W. P., Pandey, A. K., et al. 2014, *MNRAS*, 443, 1614
- Panwar, N., Samal, M. R., Pandey, A. K., et al. 2017, *MNRAS*, 468, 2684
- Pfalzner, S. 2011, *A&A*, 536, A90
- Preibisch, T., & Feigelson, E. D. 2005, *ApJS*, 160, 390
- Preibisch, T., Flaischlen, S., Gaczkowski, B., Townsley, L., & Broos, P. 2017, *A&A*, 605, A85
- Reggiani, M., Robberto, M., Da Rio, N., et al. 2011, *A&A*, 534, A83
- Rodríguez-Ledesma, M. V., Mundt, R., & Eisloffel, J. 2010, *A&A*, 515, A13
- Rosvick, J. M., & Majaess, D. 2013, *AJ*, 146, 142
- Salpeter, E. E. 1955, *ApJ*, 121, 161
- Samal, M. R., Pandey, A. K., Ojha, D. K., et al. 2012, *ApJ*, 755, 20
- Samal, M. R., Zavagno, A., Deharveng, L., et al. 2014, *A&A*, 566, A122
- Scholz, A. 2012, *MNRAS*, 420, 1495
- Sharma, S., Pandey, A. K., Ogura, K., et al. 2008, *AJ*, 135, 1934
- Sharma, S., Pandey, A. K., Borissova, J., et al. 2016, *AJ*, 151, 126
- Sicilia-Aguilar, A., Hartmann, L. W., Hernández, J., Briceño, C., & Calvet, N. 2005, *AJ*, 130, 188
- Siess, L., Dufour, E., & Forestini, M. 2000, *A&A*, 358, 593
- Skiff, B. A. 2014, *VizieR Online Data Catalog*, 1
- Slesnick, C. L., Hillenbrand, L. A., & Carpenter, J. M. 2004, *ApJ*, 610, 1045
- Stahl, O., Wade, G., Petit, V., Stober, B., & Schanne, L. 2008, *A&A*, 487, 323
- Sterzik, M. F., & Durisen, R. H. 2003, *A&A*, 400, 1031
- Stetson, P. B. 1987, *PASP*, 99, 191
- Stolte, A., Brandner, W., Grebel, E. K., Lenzen, R., & Lagrange, A.-M. 2005, *ApJL*, 628, L113
- Sugitani, K., Fukui, Y., & Ogura, K. 1991, *ApJS*, 77, 59
- Sung, H., & Bessell, M. S. 2010, *AJ*, 140, 2070
- Sung, H., Sana, H., & Bessell, M. S. 2013, *AJ*, 145, 37
- Tan, J. C., Krumholz, M. R., & McKee, C. F. 2006, *ApJL*, 641, L121
- Tobin, J. J., Hartmann, L., Furesz, G., Mateo, M., & Megeath, S. T. 2009, *ApJ*, 697, 1103
- van Dokkum, P. G., & Conroy, C. 2010, *Nature*, 468, 940
- Vázquez-Semadeni, E., González-Samaniego, A., & Colín, P. 2017, *MNRAS*, 467, 1313
- Wang, P. F., Chen, W. P., Lin, C. C., et al. 2014, *ApJ*, 784, 57
- Yang, J., & Fukui, Y. 1992, *ApJ*, 386, 618